9fabricating methods (14). By applying laser processing technology, precise fabrication of object configurations could be easily achieved (15-16). Accurate porous structure with precise pore diameter and interval could be obtained by laser drilling which has a potential to introduce capillary vessels formation into its volume.

In this study, we have developed a pierced porous tube of nonwoven chitosan mesh by electro spinning and laser drilling processes. We evaluated its efficacy as peripheral nerve bridging conduit by implanting it to rat's sciatic nerve defect. The correlation of pore density and revascularization extent as well as the influence of revascularization level to peripheral nerve regeneration was investigated.

2. Materials and methods

2.1 Conduit fabrication

a) Fabrication of nonwoven chitosan conduit:

The nonwoven chitosan mesh tube at the size of 12mm in length, 1.2 mm in inner diameter and 0.3~0.5 mm in wall thickness was prepared by electro spinning method (17-18). Chitosan solution was prepared by adding 0.8 g of chitosan powder (HOKKAIDO SODA Co., Japan) with the deacetylation rate at 90% to 10 mL of trifluoroacetic acid (TFA) (0.5mol/L, TCI, Japan) and incubating at 50°C overnight. 2.5 mL of methylene chloride (MC) (DOJINDO, Japan) was then added to this mixture and glass filtered (6.4 w/v % chitosan). For electro spinning, the chitosan-TFA-MC solution was filled in a plastic syringe fitted with a 17-mm-long needle with an inner diameter of 0.5 mm. A high voltage power supply provided a potential of 20–30 kV at a distance of 10–20 cm between the needle tip (anode) and the collector (cathode), a 100 mm thick rotating stainless drum with the linear rate at 0.52 m/s (100 rpm). A positive-charged jet ejected from the syringe at a rate of 2–8 mL/h was sprayed onto the negative-charged collector (Fig.1). Nonwoven Chitosan mesh constituted by numerous randomly crossed nano/micro fibers was formed on the drum surface, the peak (>50%) of the distribution of fiber diameters was between 200 to 600 nm (10). Obtained mesh with a thickness of 0.02 mm was carefully unrolled from the drum, reeled on a stainless bar with the diameter of 1.2 mm and immersed in 28% aqueous ammonia at room temperature overnight to neutralize the chitosan-TFA-MC. After being washed with distilled water at room temperature for 2 h, it was dipped into 100 v/v% ethanol for 3 min. As a result of slight shrinkage of the chitosan fiber, slim but sufficient clearance occurred between the bar and the tube; thus, the chitosan mesh tube was easily removed from the bar. The completed chitosan mesh tube had an inner diameter of 1.2 mm; an outer diameter of 2.0 mm and a length of 12 mm. Twenty-seven samples in total were made for further evaluations.

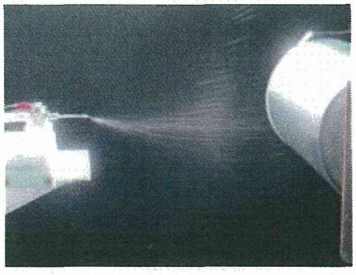

Fig. 1: Fabrication of nonwoven chitosan mesh by electrospinnning. A positive-charged jet of chitosan solution ejected from the syringe distributed onto the negative-charged drum collector. Nonwoven Chitosan mesh constituted by numerous randomly crossed nano/micro fibers was formed on the drum surface.

b) Laser drilling:

An YVO4 SHG green Laser Marker with the working wavelength of 532nm

(MD-S9900A Series, KEYENCE, Tokyo, Japan) was employed to perforate holes on the nonwoven chitosan tube wall precisely. After several tests of different settings (LE:0~100%, IT: 50~300ms), Laser Energy (LE) set at 50% and Impact Time (IT) at 150 ms were found proper for achieving stable penetrating pores. 10 pores at the size of 200 μm were punched linearly with the interval of 1mm to each other along the tube axis. Eleven samples were processed 2 lines of pores oppositely, 11 samples were processed 4 lines of pores centrosymmetricly. All samples were sterilized before animal implantation by immersion in 70% alcohol for 24 hours followed by PBS rinse.

2.2 Scanning electron microscopy

Laser drilled nonwoven chitosan conduits were dried in a critical point drying apparatus (hcp-2, Hitachi, Tokyo, Japan) with liquid CO_2, coated with platinum in an ion-sputter coater (E-1045, Hitachi, Tokyo, Japan) and observed by scanning electron microscopy (SEM) (Model S-4500, Hitachi, Tokyo, Japan). The average pore size was calculated on SEM images taken from different samples in each group, N=3 respectively.

2.3 Animal implantation

Following experiments were carefully conducted in accordance with the Guidelines for Animal Experimentation (Tokyo Medical and Dental University) as well as the National Institutes of Health (NIH) guide for the care and use of laboratory animals (Eighth Edition).

Female Wistar rats weighed 180–200 g were anesthetized with an intraperitoneal injection of sodium pentobarbital (50 mg/kg body weight). The right sciatic nerve was exposed and a 10 mm long section was excised at the center of the thigh. Experimental grafts at the length of 12 mm were implanted by end to end suturing with two sutures (8-0 monofilament nylon) at each junction (Fig. 2). Following groups were set: 1) Nonwoven chitosan conduit, 2) Nonwoven chitosan conduit with 2 lines of micro pores, 3) Nonwoven chitosan conduit with 4 lines of micro pores, 4) Isograft which is harvested from isogenic rat and considered having the nearest function of human autograft. Sample number (N) was 8 in the 2 groups with pore drilled and 5 in the left 2 control groups. Muscle and skin incision was closed with sutures of 4-0 monofilament nylon. The whole procedure was conducted under a surgical microscope (OME-9000, Olympus, Tokyo, Japan) and strictly following the standards of surgical aseptic manipulation.

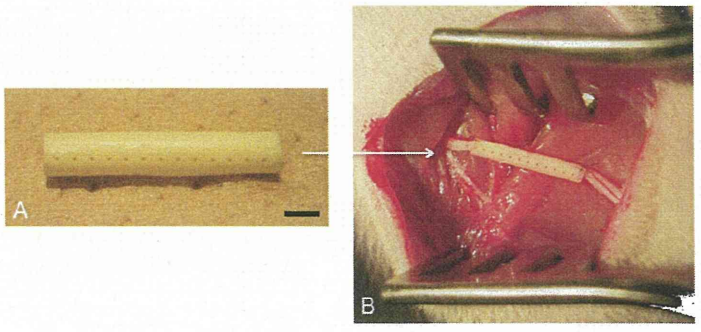

Fig. 2: A close (A) and intraoperative view (B) of the laser drilled nonwoven chitosan conduit. The conduit is 12 mm long and has 0, 2 or 4 lines of pores; every line contains 10 pores with the interval of 1mm (A). It is implanted by end to end suturing with two sutures of 8-0 monofilament nylon at each junction (B). Scale bar: 2mm

2.4 Functional test

Frey hair test (19) was applied for evaluating the final nerve function recovery before nerve harvest 12 weeks after operation (N=5 in each group). Experimental rats were

placed on a wire mesh plate and allowed to calm down. A series of Nylon monofilaments (Touch-Test Sensory Evaluator, North Coast Medical, CA) were used to stimulate the sole of the hind feet from below. The size of the monofilament was recorded when a paw withdrawal or lick reaction was repeatedly observed. Stimulating load was from No. 3.84 to 5.07, and stimulating time was 5 seconds per operation. Both sides were tested and the results were calculated using the following formula:
(Result of experimental side - Result of the normal side) / Result of the normal side

2.5 Electrophysiological evaluation

Electrophysiological evaluation was performed before animal sacrifice at 12 weeks post implantation (N=5 in each group). Under anesthesia with ketamine (80 mg/kg, intraperitoneal injection), the right sciatic nerve interposed by implant was carefully re-exposed and detached from surrounding tissues. Two recording needle electrodes were placed in the anterior tibialis muscle and the sciatic nerve was stimulated by two hook wire electrodes connected with DC electrical stimulator (Neuropack S1 MEB-9100, Nihon Kohden Co., Japan). Stimulation was set at 1 Hz in rate, 1.8 mA in intensity and 0.2 ms in duration. An earth electrode was also placed in surrounding muscle tissue to remove interference signals from surrounding tissue conduction. The stimulation was repeated for 20 times and accumulated compound action potentials (CAPs) were recorded, from which the evoking latency and the peak amplitude were measured and calculated as following formula:
| Result of experimental side - Result of the normal side |/ Result of the normal side

2.6 Histological evaluation

To verify the ingrowth of neo blood vessels through the opening pores of the conduit wall, 3 rats in both laser drilled groups were euthanized by intraperitoneal injection of overdosed sodium pentobarbital at 4 weeks after implantation. The implanted conduits were carefully harvested and the pores were observed under a surgical microscope. The conduits were then fixed in 10% formalin neutral buffer, dehydrated and embedded in paraffin, sliced longitudinally through the pores to 4 μm thick sections, followed by staining with Hematoxylin-eosin (HE). These slices were examined under a light microscope (BX51, Olympus Co., Tokyo, Japan).

For histological analysis of regenerated nerve and vessel tissue, 12 weeks after implantation 20 rats (5 from each group) were sacrificed by administering overdosed pentobarbital intraperitoneally. Implanted samples and 5 healthy nerves from opposite side were harvested and fixed in 2.5 vol. % glutaraldehyde in 0.1 M phosphate buffer, followed by post-fixation of 1% OsO4 in 0.1 M phosphate buffer. Then they were rinsed and dehydrated in a graded ethanol series, and embedded in Epon 812 resin. The mid-portions of the specimens were cut into thin cross-sections of 1 μm thickness with an ultra-microtome (EM UC6, Leica Microsystems, Wetzlar, Germany), stained with 0.5 % toluidine blue, and observed by light microscopy.

Images of the transverse sections of the implanted conduits, isografts and normal nerves were captured for the measurements of regenerated nerves by following parameters; axon diameter (minimum), density (number/mm^2) as well as vessel diameter (minimum) and density (number/mm^2). The image analyzing software, Image Pro Plus 6.0 (Media Cybernetics, Inc. MD, USA) was employed for the task.

2.7 Statistical analysis

An ANOVA, Turkey-Kramer Post-hoc test, was applied to calculate the significance of differences between mean values for each parameter. A p value less than 0.05 was considered statistically significant (20).

3. Results

3.1 Micro structure of the conduit

SEM images (Fig. 3) revealed that the wall of the conduit was constructed by overlapped thin mesh layers; every single layer was constituted by randomly crossed chitosan fibers sized from dozens of nanometers to almost 2 micrometers, Interspace between the fibers connected with each other and distributed throughout the structure resulting in a fibrous porous architecture similar to extra cellular matrix (ECM). The laser-drilled pores perforated the whole mesh layers with smooth fused edges. Average pore size was calculated at 200±12 μm and the distance between the centers of 2 neighbored pores was 1±0.04 mm.

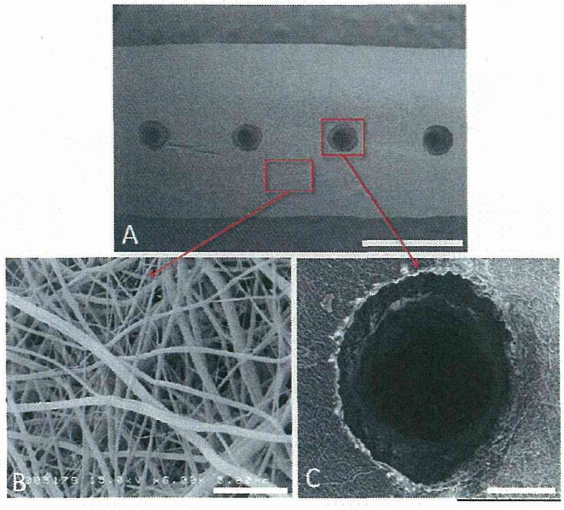

Fig. 3: SEM views of laser drilled nonwoven chitosan conduit. The conduit wall was constructed by many randomly crossed chitosan fibers sized from dozens of nanometers to almost 2 micrometers (B). (C) showed an amplified perforating pore, smooth fused edges of several nonwoven mesh layers could be seen. Average pore size was calculated at 200±12 μm. Scale bars in A, B and C is 1mm, 5 μm and 100 μm respectively.

3.2 Functional recovery

Von Frey hair test in rats records the reaction to a certain tactile stimulation, its value relates to both sensory and motor nerve function of the lower limb (19). It is easy performable and highly reliable compared to other functional tests. The result of Von Frey hair test was shown in (Fig. 4); functional loss after 12 weeks remained in approximately 15% in all experimental groups, Isographs showed a slight improvement yet statistical difference was not detected.

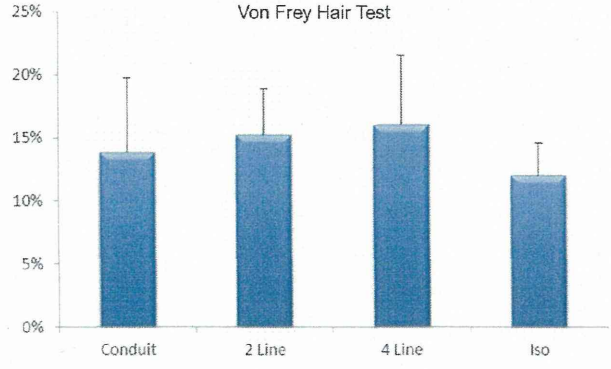

Fig. 4: Results of Von Frey hair test. Functional loss after 12 weeks remained in approximately 15% in

all experimental groups, Isographs showed a slightly better result yet statistical difference was not detected.

3.3 Electrical conductivity of regenerated nerve

CAPs latency is related to nerve conduction velocity, it is considered as a parameter of maturation; when myelinated axons increase it shortens. And amplitude reflects the total number of regenerated axons, when the number of regenerated axons grows it increases (21-22). A similar pattern was obtained with the 2 parameters in our results; conductive function loss remained about 35% after 12 weeks in conduits implanted groups without much difference between each other, Isografts receives the best results at approximately 23%, but no statistical significance was found (Fig. 5).

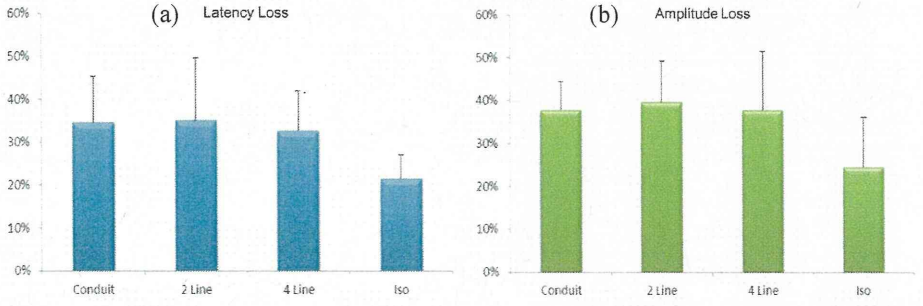

Fig. 5: Results of electro conductivity measurements. A similar pattern was obtained with either the latency (a) or the amplitude (b): conductive function loss remained about 35% after 12 weeks in conduits implanted groups without much difference between each other, Isografts receives the best results at approximately 23%, but no statistical significance was found.

3.4 Histomorphometric analysis of regenerated axon and vessel

Samples harvested at 4 weeks after implantation showed that many small vessels were passing through the pierced pores in a radial pattern (Fig. 6a). Sections cut longitudinally at the pores showed blood vessels penetrated through the pores from outside with some accompanied granulation tissue (Fig. 6b, 6c).

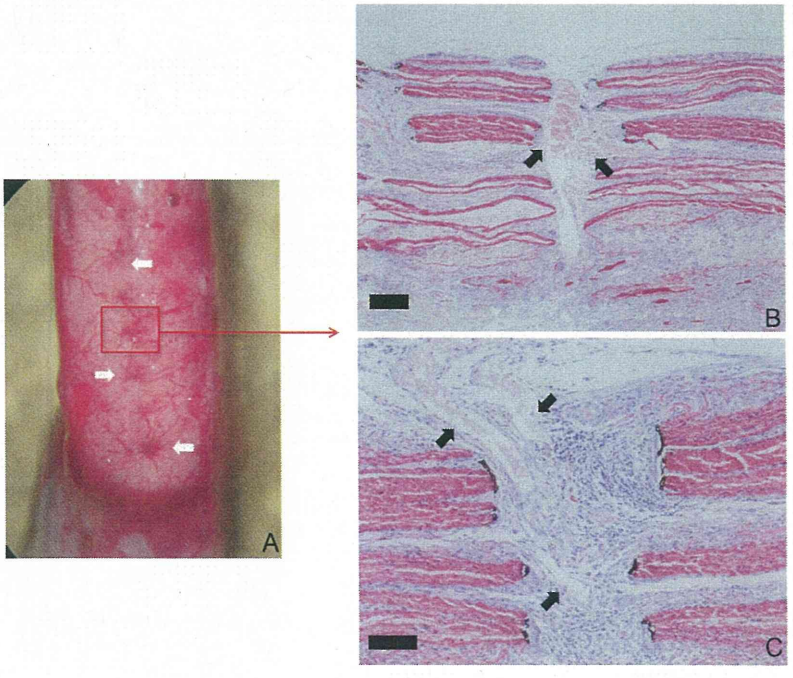

Fig. 6: Gross (A) and histological view (B, C) of the pore-drilled sample harvested at 4 weeks after

implantation. Many small vessels (white arrows in A) were entering the perforating pores in a radial pattern, blood vessels (black arrows in B, C) from outside passed through the pores with some accompanied granulation tissue. HE stain, scale bars in B, C is 200 μm and 100 μm.

Thin Epon sections of samples harvested at 12 weeks post operation revealed that all experimental groups presented vigorous axon regeneration; in the non-pore conduit group, a large number of myelinated axons with various sizes distributed in the lumen with a condensed center (Fig. 7a). Meanwhile, in pore-drilled groups (either in 2 lines or in 4 lines) regenerated axons tended to form fasciculi with endoneurium-like connective tissue sheaths surrounded. Filling of connective fibrous tissue was found very mild and displayed no difference with non-pore group (Fig. 7b, 7c). However, the isograft group presented the most intensive axon regeneration that occupied all the graft cross-sectional area (Fig. 7d).

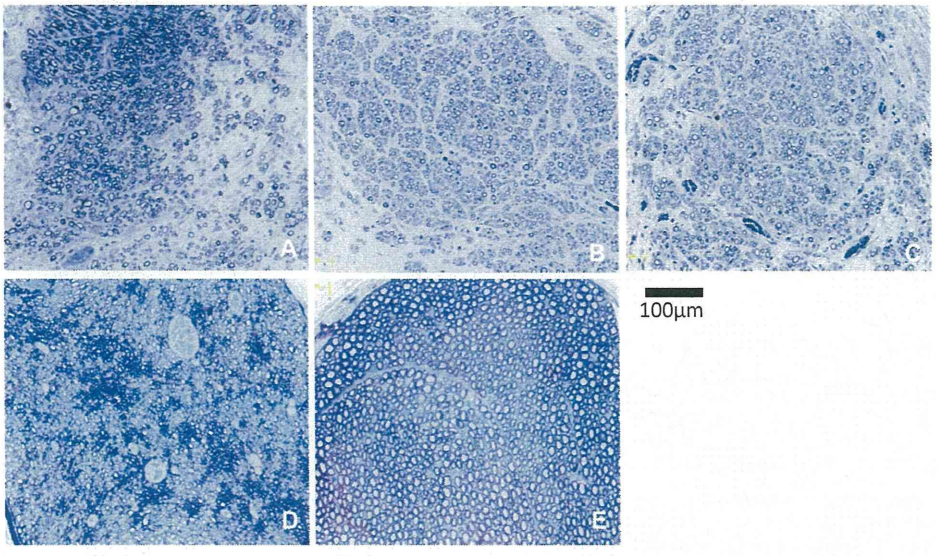

Fig. 7: Transactional view of the midpoint of samples harvested at 12 weeks after implantation. Samples are arrayed from A-E in following group order: non-pore, 2-line pores, 4-line pores, isograft and normal nerve. All experimental groups presented vigorous axon regeneration, in the non-pore conduit group (A), a large number of myelinated axons with various sizes distributed in the lumen with a condensed center; in pore-drilled groups (B, C) regenerated axons tended to form fasciculi with endoneurium-like connective tissue sheaths surrounded; the isograft group (D) presented the most intensive axon regeneration that occupied all the graft cross-sectional area. Epon thin section stained with toluidine blue.

Vessel counting indicated that the average diameter of neovascularized vessels inside the grafts varied from 7 to 13 μm, pore-drilled conduits had a tendency to present larger vessels than the other groups, yet there was no statistical significance (Fig. 8a). However, the results of vessel density measurement showed a gradient increase of vessel density in the order of non-pore conduit, conduit with 2 lines of pores, conduit with 4 lines of pores, Isograft and normal nerve. There were significant differences between the nerve conduits and Isograft or normal nerve, but with more pores opened the significance decreased, there was no significant difference between conduit with 4 lines of pores and Isograft (Fig. 8b). The effect of introducing blood vessels into lumen regenerating space by drilling perforating pores was confirmed.

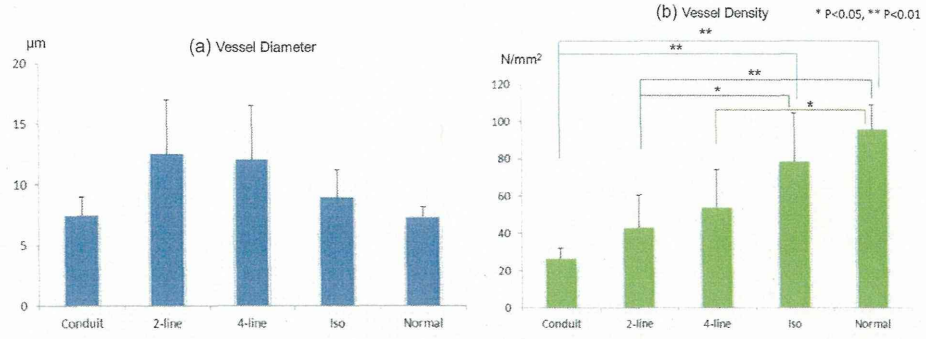

Fig. 8: Results of vessel measurements after 12 weeks of implantation. Vessel diameter was shown in (8a), they varied from 7 to 13 μm, conduits with pores had a tendency to present larger vessels than the other groups, yet there was no statistical significance. Vessel density was shown in (8b), a gradient increase of vessel density was presented in the order of non-pore conduit, conduit with 2 lines of pores, conduit with 4 lines of pores, Isograft and normal nerve. There were significant differences between the nerve conduits and Isograft or normal nerve, but with more pores opened the significance decreased, there was no significant difference between conduit with 4 lines of pores and Isograft.

The axon analysis suggested that there were no significant differences of axon size in all grafted groups; Average axon diameters from grafted groups were at 1.6 to 1.7 μm, reached approximately half the size of normal nerve (3.1 μm) at 12 weeks post operation (Fig. 9a). Meanwhile with regard to axon density, Isograft showed an outstanding abundance with the number of $5.1*10^4/mm^2$, leave the other groups far behind with their value at about $2.7*10^4/mm^2$. No differences were showed in the rest groups; however the slightly low number of normal nerve in density was considered rising from its large axon size (Fig. 9b).

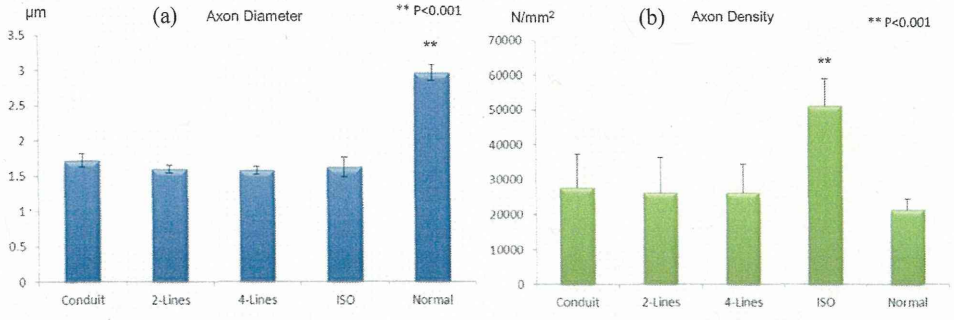

Fig. 9: Results of axon assessments at 12 weeks after implantation. Axon size was shown in (9a), there were no significant differences of axon size in all grafted groups, and they reached approximately half the size of normal nerve ($P<0.001$). Axon density was shown in (9b), isograft showed an outstanding abundance, leave the other groups far behind ($P<0.001$). No differences were found in the rest groups.

4. Discussions

In recent years, electrospinning has been extensively used to construct tissue-engineered scaffolds; it is a simple fabrication process that can easily produce nanofibrous scaffolds which are a suitable environment for cell attachment and proliferation due to their mimetic topographical features to extra cellular matrix (ECM) (23). Many reports including our previous research have demonstrated the advantages of inducing nanofiber orientation on peripheral nerve regeneration (10, 24-26), the nerve conduits fabricated by nonwoven mesh of aligned nanofibers showed better guidance of neurite ingrowth resulting in matched nerve regeneration with isograft. The reason we didn't apply

oriented nanofibrous chitosan mesh conduit in this study is from the concern that it is more convenient for a negative control to receive moderate results, to display the power of the factors that we are really interested in, which in this study is the function of perforating pores.

The regrowth of new blood vessels into tissue defects, in term of neovascularization, plays a crucial role in tissue regeneration and repair. One of the major reasons that regenerative tissue in large volume still remained a big challenge is the difficulty of guaranteeing rapid and sufficient neovascularization to support the whole regenerating process simultaneously. Several approaches to enhance revascularization were proposed like seeding of endothelia, administrating of vascular growth factors (VEGF, FGF), and stimulating slight inflammatory reaction accompanied with angiogenesis by biochemical reagents (27-30), none of them is easily accomplishable. Compared to dense biomaterials, porous bioscaffolds with interconnected inner pores provide better tissue ingrowth and integration as well as faster degeneration (31-34). Because body tissues have the tendency to fill up defect cavities with granulation tissue accompanied by neovascularization, it is reasonable to consider that through introducing perforating pores to a chamber structure inside body, the lumen contents could receive more vascular supply from surrounding tissues, and when the pore size is controlled properly the infiltration of fibrous tissue could be inhibited at a low level.

There are many literatures concerning the influences of pore sizes with different porous biomaterials (35-37). Pore sizes at 200-300 μm were considered favoring neovascularization (38-39), pore sizes of <200 μm were found to be watertight hindering liquid circulation (40) and pores of <100 μm only lead to ingrowth of single cell types instead of building up new tissues (41-43). For the accurate process of pore opening, we applied laser drilling technology which has the advantages of precision, cleanness and efficiency. We determined the pore size at 200 μm for 2 reasons: it is reported favoring neovascularization but not large enough to induce mass unfavorable fibrous tissue; after several tests of the Laser Marker, we found the minimal energy and duration setting to ensure an even penetrating pore through the whole chitosan mesh wall gave the pore size at about 200 μm. No more than 4 lines of pores (40 pores/conduit) were drilled is because of the worries of reducing conduit mechanical intensity and promoting infiltration of fibrous connective tissue.

Our grafting results suggested that by introducing perforating pores, blood supply from surrounding environment was enhanced with small vessel ingrowth and the effect depended on pore density. For peripheral nerve conduit, wall pore size at 200 μm with the density of 40/cm didn't cause obvious fibrous tissue invasion that hindering nerve regeneration. Accompanying the improved vascularization, enhancement of axon regeneration was not shown with the parameters of axon diameter and density, but morphological changes of presenting more matured fasciculi were observed.

The reasons may lie in good function of the control group, nonwoven chitosan mesh conduit, which has permeability itself and a high compatibility to neurite elongation; and also in a relatively short graft distance that could not reveal the differences. Permeation of the mesh architecture and the blood supply from the proximal/distal stumps may support the regeneration enough in a short mesh graft at the length of 12mm. Thus a longer defect model with other nerve guidance conduit is considered to be employed in further studies.

The organization of fascicular structures of axon bunds could indicate the level of maturity and functional complexity (44, 45). Different fascicles supply specific muscles and cutaneous areas, fascicularization and topography has substantial clinical relevance in nerve functions (46-49). In this study our open porous conduits not only promoted vessel ingrowth but also provided the accompanying connective tissue which facilitates the formation of fascicular sheaths, resulting in more matured histological view with the feature

of noticeable minifascicle formation. So the pore opened conduits were considered to exhibit a more natural fashion of compound tissue regeneration.

Isograft's ascendancy comes not only from the abundance of revascularization but also from the numerous guidance channels of residual basement membrane which contains many neural adhesion molecules like Laminin and Integrin. This is partially proved in our previous study with laminin coated chitosan nonvowen conduit which received comparable results with Isograft (50).

5. Conclusion

By inducing perforating pores to chitosan nonwoven conduit with laser process, conduit revascularization was improved without obvious fibrous tissue infiltration by vessel ingrowth from surrounding tissue through the pores. However except for the maturation of fasciculi, contemporary major nerve regenerative improvements were not observed. Perforating pores may help long conduits without permeability more instead of short permeable conduits.

Acknowledgements

The nonwoven chitosan mesh conduits were kindly provided by Hokkaido Soda Co., Ltd., Hokkaido, Japan. And the laser-drilling processing is supported by Keyence Corp., Tokyo, Japan.

References

1. Kemp SW, Syed S, Walsh W, Zochodne DW, Midha R. Collagen nerve conduits promote enhanced axonal regeneration, schwann cell association, and neovascularization compared to silicone conduits. Tissue Eng Part A. 2009 Aug; 15(8):1975-88.
2. Hashimoto T, Suzuki Y, Kitada M, Kataoka K, Wu S, Suzuki K, Endo K, Nishimura Y, Ide C. Peripheral nerve regeneration through alginate gel: Analysis of early outgrowth and late increase in diameter of regenerating axons. Exp Brain Res 2002; 146:356–368.
3. Suzuki Y, Tanihara M, Ohnishi K, Suzuki K, Endo K, Nishimura Y. Cat peripheral nerve regeneration across 50 mm gap repaired with a novel nerve guide composed of freeze-dried alginate gel. Neurosci Lett 1999; 259:5–78.
4. Itoh S, Suzuki M, Yamaguchi I, Takakuda K, Kobayashi H, Shinomiya K, Tanaka J. Development of a nerve scaffold using a tendon chitosan tube. Artif Organs 2003; 27: 1079-1088.
5. Mackinnon SE, Dellon AL. Clinical nerve reconstruction with a bioabsorbable polyglycolic acid tube. Plast Reconstr Surg 1990;85:419–24.
6. Toba T, Nakamura T, Shimizu Y, Matsumoto K, Ohnishi K, Fukuda S, Yoshitani M, Ueda H, Hori Y, Endo K. Regeneration of canine peroneal nerve with the use of a polyglycolic acid-collagen tube filled with laminin-soaked collagen sponge: A comparative study of collagen sponge and collagen fibers as filling materials for nerve conduits. J Biomed Mater Res 2001; 58:622–630.
7. Giraudguille MM. Fine-structure of the chitin protein system in the crab cuticle. Tissue Cell 1984;16:75–92
8. Yamaguchi I, Itoh S, Suzuki M, Sakane M, Osaka A, Tanaka J. The chitosan prepared from crab tendon I: the characterization and the mechanical properties. Biomaterials 2003;24: 2031–2036.
9. Prabhakaran MP, Venugopal JR, Chyan TT, Hai LB, Chan CK, Lim AY, Ramakrishna S. Electrospun biocomposite nanofibrous scaffolds for neural tissue engineering. Tissue Eng Part A. 2008 Nov;14(11):1787-97.
10. Wang W, Itoh S, Matsuda A, Ichinose S, Shinomiya K, Hata Y, Tanaka J. Influences of mechanical properties and permeability on chitosan nano/microfiber mesh tubes as a

scaffold for nerve regeneration. J Biomed Mater Res A 2008 Feb; 84(2):557-66
11.Wang W, Itoh S, Yamamoto N, Okawa A, Nagai A, Yamashita K Enhancement of nerve regeneration along a chitosan nanofiber mesh tube on which electrically polarized beta-tricalcium phosphate particles are immobilized. Acta Biomater. 2010 Oct;6(10):4027-33. Epub 2010 May 6.
12. Soker S, Machado M, Atala A. Systems for therapeutic angiogenesis in tissue engineering. World J Urol. 2000 Feb; 18(1):10-8.
13. Djonov V, Baum O, Burri PH. Vascular remodeling by intussusceptive angiogenesis. Cell Tissue. Res 2003; 314:107–117. [PubMed: 14574551]
14. Kaully T, Kaufman-Francis K, Lesman A, Levenberg S. Vascularization-the conduit to viable engineered tissues. Tissue Eng Part B Rev. 2009 Jun;15(2):159-6
15. Carruth JA. Lasers in medicine and surgery. J Med Eng Technol. 1984 Jul-Aug;8(4):161-7.
16. Ovsianikov A, Malinauskas M, Schlie S, Chichkov B, Gittard S, Narayan R, Löbler M, Sternberg K, Schmitz KP, Haverich. A Three-dimensional laser micro- and nano-structuring of acrylated poly(ethylene glycol) materials and evaluation of their cytoxicity for tissue engineering applications. Acta Biomater. 2011 Mar; 7(3):967-74. Epub 2010 Oct 25.
17. Xie J, MacEwan MR, Schwartz AG, Xia Y. Electrospun nanofibers for neural tissue engineering. Nanoscale. 2010 Jan 8;2(1):35-44.
18. Wang CY, Zhang KH, Fan CY, Mo XM, Ruan HJ, Li FF. Aligned natural-synthetic polyblend nanofibers for peripheral nerve regeneration. Acta Biomater. 2011 Feb; 7(2):634-43.
19. Bove G.Mechanical sensory threshold testing using nylon monofilaments: the pain field's "tin standard". Pain. 2006 Sep;124(1-2):13-7.
20. Kim YT, Haftel VK, Kumar S, Bellamkonda RV. The role of aligned polymer fiber-based constructs in the bridging of long peripheral nerve gaps. Biomaterials. 2008 Jul; 29(21):3117-27. Epub 2008 Apr 29
21. English AW, Chen Y, Carp JS, Wolpaw JR, Chen XY. Recovery of electromyographic activity after transection and surgical repair of the rat sciatic nerve. J Neurophysiol. 2007 Feb;97(2):1127-34. Epub 2006 Nov 22.
22. Krarup C. Compound sensory action potential in normal and pathological human nerves. Muscle Nerve. 2004 Apr;29(4):465-83.
23. Ceuna S, Tos P, Battiston B. International review of Neurobiology: Essays on Peripheral Nerve Repair and Regeneration (vol. 87). In: Chiono V, Tonda-Turo C, Ciardelli G. Artificial Scaffolds for Peripheral Nerve Regeneration p. 185-186.
24. Smith IO, Liu XH, Smith LA, Ma PX. Nanostructured polymer scaffolds for tissue engineering and regenerative medicine. Wiley Interdiscip Rev Nanomed Nanobiotechnol. 2009 Mar-Apr;1(2):226-36.
25. Biazar E, Khorasani MT, Montazeri N, Pourshamsian K, Daliri M, Rezaei M, Jabarvand M, Khoshzaban A, Heidari S, Jafarpour M, Roviemiab Z. Types of neural guides and using nanotechnology for peripheral nerve reconstruction. Int J Nanomedicine. 2010 Oct 21;5:839-52.
26. Wang W, Itoh S, Konno K, Kikkawa T, Ichinose S, Sakai K, Ohkuma T, Watabe K. Effects of Schwann cell alignment along the oriented electrospun chitosan nanofibers on nerve regeneration. J Biomed Mater Res A. 2009 Dec 15;91(4):994-1005.
27. Glotzbach JP, Levi B, Wong VW, Longaker MT, Gurtner GC The basic science of vascular biology: implications for the practicing surgeon. Plast Reconstr Surg. 2010 Nov;126(5):1528-38.
28. Nomi M, Atala A, Coppi PD, Soker S. Principals of neovascularization for tissue engineering. .Mol Aspects Med. 2002 Dec;23(6):463-83.
29. Hegen A, Blois A, Tiron CE, Hellesøy M, Micklem DR, Nör JE, Akslen LA, Lorens JB.